

Structure-based optimization of non-quaternary reactivators of acetylcholinesterase inhibited by organophosphorus nerve agents

Gianluca Santoni, Julien de Sousa, Eugenio De la Mora, José Dias, Ludovic Jean, Joel L. Sussman, Israel Silman, Pierre-Yves Renard, Richard C. D. Brown, Martin Weik, Rachid Baati, and Florian Nachon

J. Med. Chem., **Just Accepted Manuscript** • DOI: 10.1021/acs.jmedchem.8b00592 • Publication Date (Web): 20 Aug 2018

Downloaded from <http://pubs.acs.org> on August 26, 2018

Just Accepted

“Just Accepted” manuscripts have been peer-reviewed and accepted for publication. They are posted online prior to technical editing, formatting for publication and author proofing. The American Chemical Society provides “Just Accepted” as a service to the research community to expedite the dissemination of scientific material as soon as possible after acceptance. “Just Accepted” manuscripts appear in full in PDF format accompanied by an HTML abstract. “Just Accepted” manuscripts have been fully peer reviewed, but should not be considered the official version of record. They are citable by the Digital Object Identifier (DOI®). “Just Accepted” is an optional service offered to authors. Therefore, the “Just Accepted” Web site may not include all articles that will be published in the journal. After a manuscript is technically edited and formatted, it will be removed from the “Just Accepted” Web site and published as an ASAP article. Note that technical editing may introduce minor changes to the manuscript text and/or graphics which could affect content, and all legal disclaimers and ethical guidelines that apply to the journal pertain. ACS cannot be held responsible for errors or consequences arising from the use of information contained in these “Just Accepted” manuscripts.

1
2
3 Structure-based optimization of non-quaternary reactivators of
4
5
6 acetylcholinesterase inhibited by organophosphorus nerve agents
7
8

9
10 Gianluca Santoni^{a,b,§}, Julien de Sousa^{c,d,§}, Eugenio de la Mora^{a,§}, José Dias^b, Ludovic Jean^c,
11
12 Joel L. Sussman^f, Israel Silman^g, Pierre-Yves Renard^c, Richard C. D. Brown^d, Martin Weik^a,
13
14 Rachid Baati^c and Florian Nachon^{b,*}
15
16
17
18
19

20 ^a Univ. Grenoble Alpes, CEA, CNRS, IBS, F-38000 Grenoble
21
22

23 ^b Département de Toxicologie et Risques Chimiques, Institut de Recherche Biomédicale des
24
25 Armées, 91220 Brétigny-sur-Orge, France
26
27

28 ^c Université de Strasbourg, ICPEES, UMR CNRS 7515, 67087 Strasbourg, France
29
30

31 ^d University of Southampton, Department of Chemistry, Highfield, Southampton, SO17 1BJ,
32
33 United Kingdom
34

35 ^e Université de Normandie, COBRA, UMR 6014, FR 3038, Université de Rouen, INSA de
36
37 Rouen, CNRS, 76821 Mont-Saint-Aignan, France.
38
39

40 ^f Department of Structural Biology, Weizmann Institute of Science, 76100 Rehovot, Israel.
41
42

43 ^g Department of Neurobiology, Weizmann Institute of Science, 76100 Rehovot, Israel.
44
45
46
47
48
49
50
51
52
53
54
55
56
57
58
59
60

Abstract

Acetylcholinesterase (AChE), a key enzyme in the central and peripheral nervous systems, is the principal target of organophosphorus nerve agents. Quaternary oximes can regenerate AChE activity by displacing the phosphyl group of the nerve agent from the active-site, but they poorly distribute in the central nervous system. A promising reactivator based on tetrahydroacridine linked to a non-quaternary oxime is also an undesired sub-micromolar reversible inhibitor of AChE. X-ray structures and molecular docking indicate that structural modification of tetrahydroacridine might decrease inhibition without affecting reactivation. The chlorinated derivative was synthesized, and, in line with the prediction, displayed a 10-fold decrease in inhibition, but no significant decrease in reactivation efficiency. X-ray structures with the derivative rationalize this outcome. We thus show that rational design based on structural studies permits the refinement of a new generation pyridine aldoxime reactivators that may be more effective in the treatment of nerve agent intoxication.

Introduction

Acetylcholinesterase (AChE) is found at cholinergic synapses throughout the nervous system, and at the neuromuscular junction. Its principal role is to terminate the synaptic transmission by rapid hydrolysis of the neurotransmitter acetylcholine (ACh) ¹. AChE is the principal target of organophosphate (OP) pesticides and nerve agents. Although use of nerve agents has been restricted by international conventions, they remain a serious threat, as demonstrated by the sarin attack at Khan Sheikhoun in Syria in april 2017, the assassination of Kim Jong-nam in february 2017 in Malaysia with VX and the poisoning of Serguei Skripal in march 2018 in England with a Novichok. The standard treatment for nerve agent intoxication consists of an antimuscarinic (atropine), an anticonvulsivant (usually diazepam), and a pyridinium oxime reactivator of the phosphylated AChE. Pyridinium oximes are sufficiently nucleophilic to displace the phosphyl group from AChE's active-site serine ², but despite 60 years of research ^{2, 3} they display major drawbacks in terms of bioavailability in the central nervous system ⁴ and a restricted spectrum of action and effectiveness ⁵. In particular, the permanent charge on the pyridinium severely limits passage through the blood–brain barrier (BBB) ⁶. For the bioavailability of 2-pyridinealdoxime (2-PAM) has been estimated to be only 10% of that in the bloodstream in rat brain as measured by *in vivo* microdialysis coupled with HPLC/UV ⁴. Furthermore, most reactivators are ineffective against tabun poisoning, none of them has proved to be equally effective against all other types of OP-AChE conjugates, and they are incapable of reactivating “aged” OP-AChE conjugates ⁵.

Toxogonin was one the first bifunctional oximes to be synthesized and investigated ⁷. Numerous elongated ligands, containing either one or two oxime moieties at their extremities, including the Hagendorn oximes, have since been studied as AChE reactivators ⁸⁻¹⁰. Now that the crystal structures of *Tc*AChE ¹¹ and mammalian AChEs ¹² have become available, it is realized that such elongated oximes span the active-site gorge, bridging between the catalytic

1
2
3 aromatic site (CAS) and the peripheral aromatic site (PAS). However, structural studies, such
4
5 as those of Ekström and colleagues^{13, 14}, have shown that binding of oximes within the
6
7 active-site gorge of AChE is far from optimal for reactivation.
8

9
10 In an earlier study¹⁵, we reported the design, synthesis and reactivation properties of a new
11
12 class of bifunctional reactivators in which the moiety interacting with the PAS is based on
13
14 tetrahydroacridine (Figure 1). The lead reactivator molecule, **1**, reversibly inhibits AChEs in
15
16 the submicromolar range. Though it is not yet clear whether this could prejudice its *in vivo*
17
18 efficacy as a reactivator, we wished to explore ways of decreasing inhibitor potency without
19
20 concomitant loss of reactivator efficacy. First, based on crystallographic structures of
21
22 complexes of **1** with apo, nerve agent-inhibited, and carbamylated *Tc*AChE we identified the
23
24 structural basis for its high inhibitory potency. This permitted us to design an improved
25
26 molecule, reactivator **2**, that successfully prevents the binding mode responsible for the
27
28 submicromolar inhibition of the apo enzyme, without altering the reactivating capacity.
29
30 Kinetic measurements, together with structural studies, confirmed the success of our strategy.
31
32
33
34
35
36
37
38
39
40
41
42
43
44
45
46
47
48
49
50
51
52
53
54
55
56
57
58
59
60

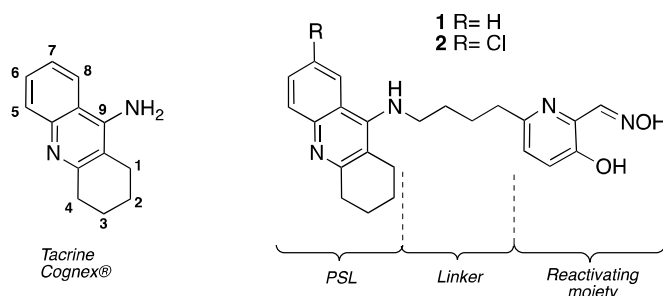
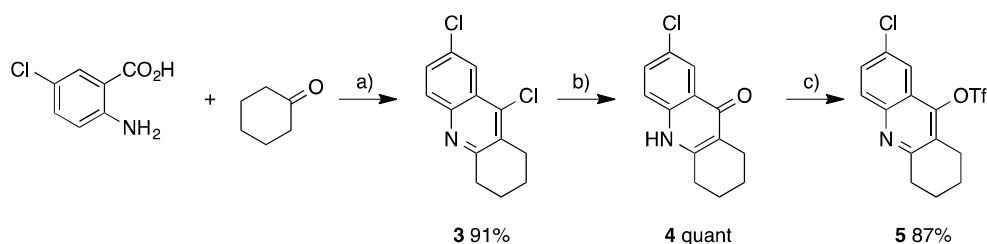


Figure 1 Chemical structures of tacrine and uncharged hybrid reactivators **1** and **2**.

Results and discussion

Chemistry

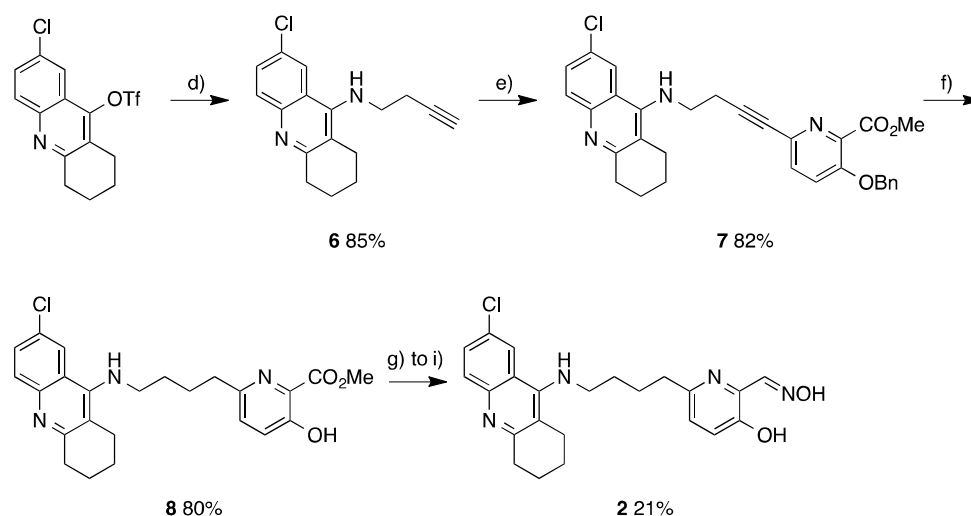
Following the route established by Baati and co-workers¹⁵, the synthesis of the reactivator, **2**, is herein described. Our initial efforts focused on the synthesis of the PSL scaffold. *N*-Alkylation of 9-aminotacrine proved not to be a reliable method^{16, 17}. A new strategy was devised that involved use of a novel electrophilic compound, 7-chloro-1,2,3,4-tetrahydroacridin-9-yl trifluoromethanesulfonate, **5** (Scheme 1)¹⁸. Starting from commercially available 5-chloroanthranilic acid, 7,9-dichloro-1,2,3,4-tetrahydroacridine, **3**, was obtained by Lewis Acid-mediated intermolecular cyclodehydration with cyclohexanone. This intermediate, **4**, was subsequently hydrolyzed using glacial acetic acid at 200 °C in a sealed tube. This two-step synthetic sequence proved to be superior to the more frequently reported direct condensation reactions of anthranilic acids and cycloalkanone via azeotropic distillation of water¹⁹. Then, triflation allowed isolation of the desired 7-chloro-1,2,3,4-tetrahydroacridin-9-yl trifluoromethanesulfonate, **5**, in an excellent overall yield (Scheme 1).



Scheme 1 Synthesis of the trifluoromethanesulfonate **5**. Conditions and reagents: (a) POCl₃, cyclohexanone, Δ, 16 h; (b) AcOH, 200 °C, 24 h; (c) Tf₂O, Et₃N, CH₂Cl₂, -78 °C for 1 h then RT for 16 h.

Introduction of the linker was achieved using our optimized microwave assisted Pd-catalysed Buchwald-Hartwig amination procedure¹⁸ to afford the desired terminal alkynes in excellent yields (Scheme 2). Subsequent Sonogashira coupling with methyl 3-benzyloxy-6-bromopicolinate²⁰ proceeded well to generate the corresponding hybrid precursors. Then, a *one-pot* alkyne reduction and *O*-debenzylation under hydrogen in the presence of Pearlman's

catalyst afforded the 3-hydroxypyridine derivatives **8**. The latter was converted into the corresponding oxime using a three-step sequence involving TBS protection of the phenolic group, reduction of the methyl ester to an aldehyde function with DIBAL-H, and subsequent oxime formation by condensation with hydroxylamine (Scheme 2). The desired hybrid was thus obtained in 10 steps in an overall 7% yield.



Scheme 2 Synthesis of the hybrid reactivator **2**. Conditions and reagents: (d) 1-amino-3-butyne, Pd₂(dba)₃, (±)-BINAP, Cs₂CO₃, 1,4-dioxane, μW (100 °C, 1 h); (e) methyl 3-benzyloxy-6-bromopyridinate, Pd[PPh₃]₄, CuI, THF/Et₃N, rt, 16 h; (f) H₂ (1 atm), Pd(OH)₂/C, EtOAc, rt, 7 h; (g) TBSOTf, 2,6-lutidine, CH₂Cl₂, rt, 2 h; (h) DIBAL-H, CH₂Cl₂, -78 °C, 12 min; (i) NH₂OH.HCl, NaOAc, EtOH, Δ, 15 h.

It is noteworthy that during the synthesis of the hybrid, the phenolic TBS group was found to be quite labile, mainly due to electron deficiency of the pyridine system that determines the strength of the Si–O bond. This observation was turned to our advantage since, after the DIBAL–H reduction, a work-up using aqueous 1 M NaOH sufficed to deprotect the silyloxy intermediate, and thus avoid using a toxic fluoride-containing reagent.

X-ray structures of compound **1** in complex with *TcAChE* and with *OP/TcAChE* conjugates.

To optimize a reactivator, detailed structural information is important for designing the improved version. Both the structures of the *TcAChE-1* complex and of the NEDPA-

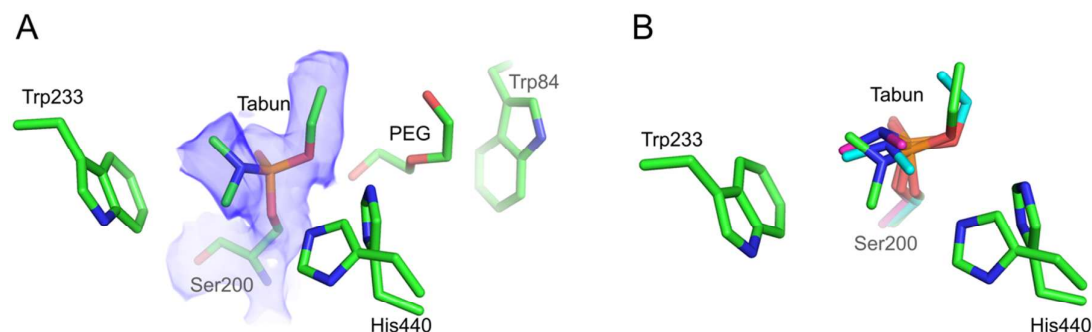
1
2
3 *TcAChE-1* ternary complex were solved in order to provide such information. Data collection
4
5 and refinement statistics for all the structures of the present article are reported in Table 1.

6
7 **Table 1** Data collection and refinement statistics. Calculated using Phenix (Adams *et al* Acta Cryst. D
8
9 2010;66:213-221). $R\text{-work} = \frac{\sum |F_o - |F_c||}{\sum |F_o|}$, F_o and F_c are observed and calculated structure factors, R-free
10
11 set uses about thousands randomly chosen reflections. Statistics for the highest-resolution shell are shown in
12
13 parentheses.

Complex	Tabun- <i>TcAChE</i>	<i>TcAChE-1</i>	NEDPA- <i>TcAChE-1</i>	<i>TcAChE-2</i>	NEDPA- <i>TcAChE-2</i>	Carbamyl- <i>TcAChE-1</i>	Carbamyl- <i>TcAChE-2</i>
PDB code	6g17	6g4m	6g4o	6g4n	6g4p	6fld	6fqn
Data Collection							
Resolution Range (Å)	45.7-2.2 (2.28-2.20)	45.91-2.63 (2.72-2.63)	58.14-2.90 (3.00-2.90)	46.3-2.90 (3.0-2.9)	45.92-2.72 (2.82-2.72)	37.32-2.40 (2.49-2.40)	37.13-2.3 (2.38-2.3)
Space group	P3121	P212121	P212121	P212121	P212121	P3121	P3121
Unit cell parameters (Å)	111.8 111.8 137.2	91.3 106.2 150.5	91.5 106.4 150.5	91.8 107.2 150.4	91.83 107.4 151.2	114.01 114.01 136.98	113.43 113.43 137.57
Total Reflections	274775 (27951)	214755 (21464)	150232 (15096)	212283 (21557)	173389 (17585)	280500 (27774)	318401 (30477)
Unique Reflections	50213 (5024)	43964 (4317)	32837 (3215)	33562 (3300)	40508 (3947)	40569 (3956)	45946 (4513)
Multiplicity	5.5 (5.6)	4.9 (5.0)	4.6 (4.7)	6.3 (6.5)	4.3 (4.5)	6.9 (7.0)	6.9 (6.7)
Completeness %	98.8 (98.5)	99.5 (99.4)	98.7 (99.1)	99.9 (99.9)	99.2 (99.9)	99.7 (97.9)	99.7 (99.7)
Mean I/sigma(I)	13.7 (2.2)	9.2 (1.9)	9.20 (2.3)	10.1 (2.9)	3.8 (0.8)	14.3 (2.2)	11.3 (2.3)
CC _{1/2}	0.99 (0.92)	0.99 (0.74)	0.99 (0.85)	0.99 (0.90)	0.95 (0.38)	0.99 (0.87)	0.99 (0.81)
Refinement							
Rwork (%)	17.5 (32.7)	19.0 (28.2)	18.5 (25.4)	19.4 (27.2)	21.0 (33.6)	18.3 (31.5)	20.5 (39.0)
Rfree (%)	21.6 (33.7)	26.5 (37.2)	26.1 (33.2)	26.6 (31.5)	28.0 (43.1)	21.4 (37.6)	23.4 (38.2)
RMS bond length	0.008	0.009	0.009	0.097	0.009	0.011	0.007
RMS bond angles	1.08	1.2	1.2	2.28	1.27	0.99	1.00
Total atoms	4784	9139	8856	9051	8679	4577	4540
Ramachandran							
favorable	96	94	92	92	92	95	94
outliers	0.19	0.28	0.47	0.19	1.0	0.19	0.76
Average B-factor (Å ²)	42.0	35	39.5	32.5	37.2	52.2	51.4

First, we solved the structure of the non-aged form of the tabun-*TcAChE* conjugate, which could serve as a template for subsequent refinements. Crystals of the conjugate were obtained by a 2-min soak of the native trigonal *TcAChE* crystals in mother liquor containing 0.5 mM

1
2
3 tabun. Figure 2 shows the similarity of this structure to those of the tabun conjugates of
4 mAChE and hAChE²¹.
5
6
7



20
21 **Figure 2** A) Structure of the non-aged tabun-*TcAChE* conjugate (pdb 6g17). Volume representation of the
22 feature enhanced map (fem) around the catalytic serine contoured at 1 σ , showing the phosphyl moiety attached
23 to Ser200. His440 is observed in two alternate conformations with equal occupancy; B) Superimposition of the
24 phosphorylated catalytic serine of non-aged tabun-*TcAChE* (pdb 6g17, green), tabun-mAChE (pdb 3dl4, cyan)
25 and the aged tabun-hAChE conjugate (pdb 2x8b, magenta). The orientation of the dimethylamino group of
26 tabun is similar in all three structures, suggesting that also in *TcAChE* aging occurs via loss of the ethyl group.
27
28
29
30

31
32 In all three structures the dimethylamino group of tabun is located in the acyl binding pocket,
33 and the O2 oxygen atom is stabilized within the oxyanion hole. These structural findings
34 support the notion that the tabun-AChE conjugate ages by O-dealkylation. The ethyl group of
35 tabun points toward Trp84, at the bottom of the gorge, thus inducing rotation of His440 to
36 adopt a non-native conformation that had been observed previously in other non-aged OP
37 conjugates^{22, 23}. The presence of the tabun moiety combined with this alternate conformation
38 of His440 reduces by 15% the solvent accessible volume of the active-site gorge with respect
39 to the native enzyme. PEG molecules from the mother liquor occupy the remaining accessible
40 volume at the bottom of the gorge and at the PAS²⁴.
41
42
43
44
45
46
47
48
49
50

51 The structure of the complex of reactivator **1** with orthorhombic *TcAChE* is shown in Figure
52 3A.
53
54
55
56
57
58
59
60

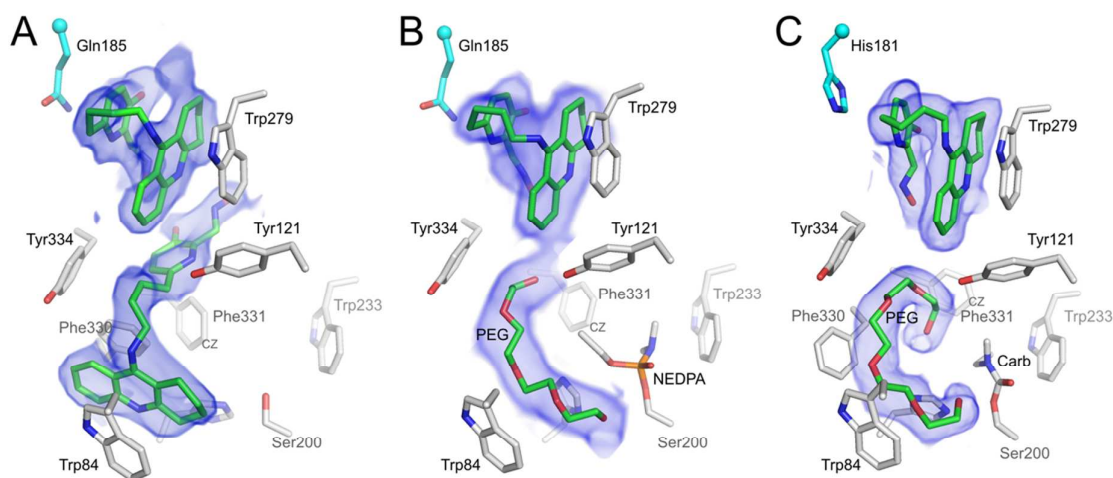


Figure 3 Crystal structures of unmodified *TcAChE* and of its conjugates complexed with **1**. Volume represents feature enhanced maps (fem) contoured at 1σ . A) *TcAChE-1* complex obtained from orthorhombic crystals (pdb 6g4m). Two copies of **1** are seen, one at the bottom of the gorge, and one at the PAS; B) NEDPA-*TcAChE-1* complex obtained from orthorhombic crystals (pdb 6g4o). A copy of **1** is seen at the PAS, and a PEG oligomer is seen alongside the phosphyl group at the bottom of the gorge; C) Carbamyl-*TcAChE-1* complex, obtained from trigonal crystals (pdb 6fld). A copy of **1** is seen at the PAS, and a PEG oligomer is seen alongside the carbamyl group at the bottom of the gorge. The binding orientation of **1** at the PAS in the 3 panels is stabilized by Gln185 or His181 (cyan) of a symmetry mate specific of the crystal packing, thus partially artefactual.

In each of the two monomers in the asymmetric unit two molecules of **1** are observed within the gorge, which displace PEG oligomers that are otherwise present in the gorge of the crystalline enzyme. One of these oligomers is located at the bottom of the gorge, near the catalytic triad. The tacrine moiety of **1** is oriented just as in the tacrine-*TcAChE* complex²⁵. The linker points towards the entrance of the gorge, with the oxime moiety positioned below the PAS. It is noteworthy that the oxime function does not lie in the plane of the pyridine, as it does in the energy-optimized molecule, but appears to be at an angle of 40° to the aromatic ring. At the PAS, a second copy of **1** is positioned such that the tacrine moiety stacks against the indole of Trp279, and the linker makes a U-turn, as a consequence of which its pyridinaldoxime ring stacks against its tacrine moiety. Indeed, the linker and the pyridinaldoxime cannot extend down into the gorge due to the presence of the first copy at

1
2
3 the CAS. The conformation of the pyridinaldoxime in the second copy seems to be stabilized
4 by interaction with Gln185 (cyan sticks in Figure 3A) of a symmetry-related copy of the
5 protein. The resolution of the structure is not high enough to permit assignment of the
6 orientation of the tacrine moiety of the second copy; thus, the aromatic and saturated rings
7 might be inverted. This holds true for all the subsequent structures presented.

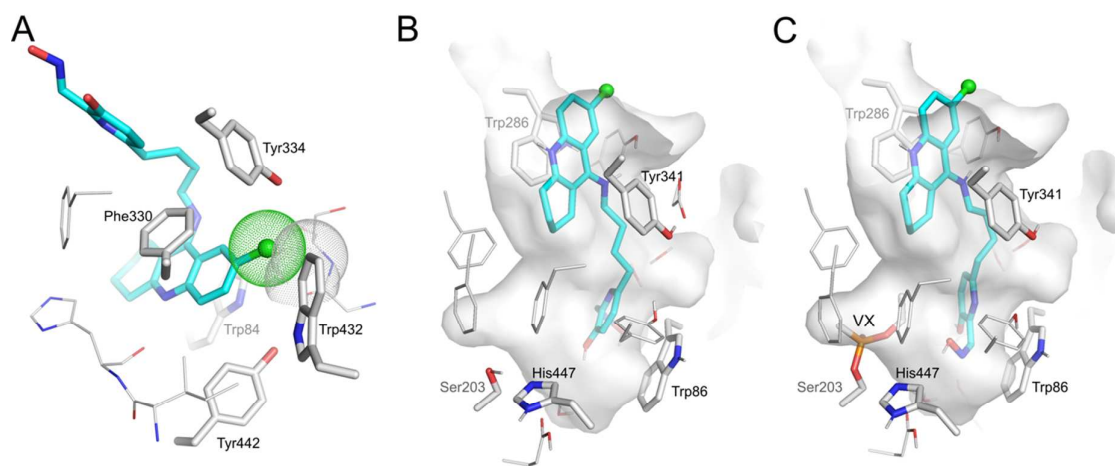
8
9
10
11
12
13 NEDPA is a *p*-nitrophenyl homolog of tabun with reduced toxicity; it is assumed, however,
14 to produce an identical AChE conjugate²⁶, thus making it a useful surrogate. We solved the
15 structure of the NEDPA-*TcAChE-1* ternary complex by successively soaking native
16 orthorombic *TcAChE* crystals in NEDPA, and then in NEDPA plus **1**, with the objective of
17 observing the complex of **1** with the conjugate prior to reactivation (Figure 3B). As we had
18 assumed, NEDPA forms an adduct identical to that obtained with tabun, with its
19 dimethylamino group located in the acyl-binding pocket. The presence of the phosphyl
20 adduct prevents the binding of **1** at the bottom of the gorge and stabilizes a PEG molecule
21 also interacting with Trp84. A copy of **1** is seen to be bound at the PAS of monomer B with
22 the pyridinaldoxime group stacked against the tacrine moiety, in a non-productive state
23 (Figure 3B), in a similar orientation to that seen at the PAS in the *TcAChE-1* complex (Figure
24 3A). However, no copy of **1** is observed at the PAS of monomer A. Instead, a large PEG
25 oligomer spans all the space from the active site to the PAS, occupying all the available space
26 (not shown).

27
28
29
30
31
32
33
34
35
36
37
38
39
40
41
42
43
44 To further explore how modification of the active-site serine impacts the binding of **1**, we
45 solved the structure of a ternary complex of **1** with carbamylated *TcAChE* obtained with a
46 trigonal crystal. Carbamylation was achieved using a rivastigmine analog, resulting in Ser200
47 being modified by an *N,N*-ethylmethyl carbamyl group. The ethyl group of the carbamyl
48 moiety induces a rearrangement of the acyl-loop with the sidechain of Phe288 being rotated
49 by 110° around χ_1 (bond CA-CB), resulting in displacement of Phe331 towards the acyl-

1
2
3 binding pocket, with its CZ atom moving 3.6 Å. The carbamyl residue significantly reduces
4 the accessible volume at the bottom of the gorge compared to the apo enzyme. Thus, a PEG
5 molecule occupies the remaining space, while a molecule of **1** occupies the PAS (Figure 3C),
6 as in the *TcAChE-1* (Figure 3B) and NEDPA-*TcAChE-1* (Figure 3C) complexes. Due to the
7 different packing of trigonal compared to orthorhombic crystals, the closest symmetry-related
8 residue stabilizing the pyridinaldoxime's conformation is His181 rather than Gln185.
9
10
11
12
13
14
15

16 Design and docking of reactivator **2**

17
18 The structural data presented above showed that the tacrine moiety of reactivator **1** can bind
19 both at the PAS and the CAS of the free enzyme. We conjectured that binding at the CAS is
20 responsible for the inhibitory potency of **1**. We wished to modify **1** so as to prevent its
21 binding at the CAS while preserving its capacity to binding at the PAS, and thus its affinity
22 for the phosphorylated enzyme. Careful inspection of the structure of the *TcAChE-1* complex
23 suggests that introducing a chlorine atom at position 7 on the tacrine moiety would create a
24 steric clash with Trp432 when the ligand was bound at the active site (Figure 4A).
25
26
27
28
29
30
31
32
33



34
35
36
37
38
39
40
41
42
43
44
45
46
47
48
49 **Figure 4** A) Model based on the structure of *TcAChE-1* complex (pdb 6g4m) showing the steric clash between
50 Trp432 and **1** in which the tacrine moiety has been modified by a chlorine atom at position 7 yielding **2**. The van
51 der Waals volumes are represented as dotted spheres; B) Docking of **2** in human AChE (pdb 4ey4); C) Docking
52 of **2** in a model of VX-inhibited hAChE (pdb 4ey4). Both docking predict that the chlorine substituent of **2**
53 prevent binding at the bottom of the gorge but permit binding at the PAS.
54
55
56
57
58
59
60

This possibility was tested by molecular docking. Both **1** and the new reactivator proposed, **2**, were docked into both native and VX-inhibited hAChE. Examination of the binding modes indicates that **2** does not bind at the CAS, but only at the PAS, thus confirming the validity of the design prediction (Figure 4B-C). The estimated binding energies for the best pose suggest that **2** is a weaker inhibitor than **1** (respectively -10.1 and -13.3 kcal/mol). Furthermore, the binding energy of **2** for VX-inhibited AChE is in the same order of magnitude than that of **1** indicating that binding to phosphorylated AChE has been preserved (respectively -13.1 and -11.7 kcal/mol).

***In vitro* evaluation of reactivators 1 and 2**

The reference oximes are 2-PAM, which is utilized by the French and US Military², obidoxime used by the German forces, and HI-6, a Hagendorn oxime, which has been investigated by the Canadian forces due to its effectiveness against soman intoxication⁸. We measured the half-maximal inhibitory concentration (IC_{50}) of the reference oximes and reactivators **1** and **2** (Table 1). Introduction of the chlorine atom reduced the affinity for the native enzyme by almost 10-fold, up to the low micromolar range. This remains 1 to 2 orders higher than the reference oximes.

Table 1 half-maximal inhibitory concentration (IC_{50}) concentration for hAChE

Reactivators	2-PAM	HI-6	Obidoxime	1	2
IC_{50} (μ M)	560 \pm 30	54 \pm 5	640 \pm 70	0.25 \pm 0.02	2.3 \pm 0.2

1 and **2** were then tested for their capacity to reactivate the conjugates of hAChE with VX, tabun, paraoxon, and the NIMP surrogate of sarin. For each of these OPs, we measured the second-order rate constant for reactivation (k_{r2}), which is the ratio of the maximal reactivation rate constant (k_r) and the apparent dissociation constant of the reactivator/phosphyl-AChE complex (K_D). These measurements were made using the Ellman

procedure, at pH 7.4 and 37 °C, viz., close to the physiological conditions^{15, 27}. The reactivation kinetics constants are reported in table 2.

Table 2 Reactivation constants of **1** and **2** at 37°C for hAChE inhibited by various OP.

	k_r (min ⁻¹)	K_D (μM)	k_{r2} (mM ⁻¹ min ⁻¹) ^a
VX			
2-PAM	0.1 ± 0.01	210 ± 60	0.51
HI-6	0.65 ± 0.03	70 ± 8	9.3
Obidoxime ^b	0.60 ± 0.05	54±12	11
1 ^b	0.72 ± 0.07	31 ± 6	22
2	0.29 ± 0.02	21.3 ± 5.1	13.6
Sarin (NIMP)			
2-PAM	0.24 ± 0.02	210±30	1.18
HI-6	1.2 ± 0.2	90 ± 34	12.9
Obidoxime	0.17 ± 0.02	500 ± 95	0.34
1	0.33 ± 0.01	20 ± 3	16.5
2	0.14 ± 0.01	11.5 ± 3.1	12.2
Tabun			
2-PAM	0.15 ± 0.03	790 ± 190	0.2
HI-6	0.05 ± 0.005	200 ± 40	0.24
Obidoxime ^b	0.04 ± 0.006	250 ± 110	0.16
1 ^b	0.021 ± 0.001	7.1 ± 1.5	3
2	0.12 ± 0.01	10.4 ± 2.6	11.5
Ethyl paraoxon			
2-PAM	0.054 ± 0.006	400 ± 80	0.14
HI-6	0.09±0.01	800 ± 140	0.1
Obidoxime	0.29 ± 0.02	550 ± 90	0.53

1 ^b	0.111 ± 0.002	3.6 ± 0.2	31
2	0.11 ± 0.01	5.7 ± 1.7	19.2

^a $k_{r2} = k_r/K_D$ ^b from Kliachyna et al ¹⁵.

Reactivator **2** outperformed 2-PAM, HI-6 and obidoxime. For the VX-hAChE conjugate, **2** is 27- more effective than 2-PAM and slightly better than HI-6 and obidoxime, respectively 1.5- and 1,2-fold. While it remained slightly less effective than reactivator **1**, reactivator **2** exhibited higher affinity (1.4-fold) for VX-AChE. For paraoxon-hAChE, **2** is 140- , 190- and 36-fold more effective than 2-PAM, HI-6 and obidoxime respectively. Towards the OP-hAChE conjugate obtained with the sarin surrogate, NIMP, **2** is 10- and 36-fold more effective than 2-PAM and obidoxime. It displayed effectiveness similar to that of HI-6, which is known to be quite efficient against sarin intoxication ⁵.

Quite remarkably, reactivator **2** exhibited the best reactivation potency for tabun poisoning. It is 4-fold more effective than **1**, and about 60-fold more effective than 2-PAM, HI-6 and obidoxime. The conjugates formed with tabun are known to be amongst the most difficult to reactivate, due to the weak electrophilicity of the phosphyl moiety and to the steric hindrance imposed on the phosphorus atom by the dimethylamino group in the hAChE-tabun adduct ²¹, ²².

Globally, this kinetic evaluation reveals that **2** is a very promising reactivator candidate with broad spectrum activity, and significantly less inhibitory potency than **1** in line with docking results. Based on the k_r and K_D constants reported in table 2, **2** attains theoretical clinically relevant concentrations for each OP evaluated by contrast to **1**, HI-6, obidoxime and especially 2-PAM (See Supplementary Information). Noteworthy, and similarly to what is measured for 2-PAM, HI-6 and obidoxime, the K_D of **2** for the different nerve agent conjugates is in the same order of magnitude as the IC_{50} for hAChE. This suggests that **2** should have a therapeutic window comparable to these oximes in regard to their side effects related to hAChE reversible inhibition.

X-ray structures of reactivator **2** in complex with *TcAChE* and conjugates.

The structure of the *TcAChE*-**2** complex is shown in Figure 5A. Each of the two monomers in the asymmetric unit, contains one molecule of **2** bound at the PAS, with aromatic stacking of Trp279, the tacrine moiety, and the pyridinaldoxime ring, as already observed for **1**. No copy of **2** can be seen at the bottom of the active site gorge, presumably due to the steric hindrance imposed by the chlorine substituent, as predicted. Despite the fact that PEG oligomers are not detected within the active site, the pyridinaldoxime does not point down the gorge as predicted by docking. The pocket formed at the gorge entrance by a symmetry-related protein copy probably dictates the orientation of the pyridinaldoxime moiety.

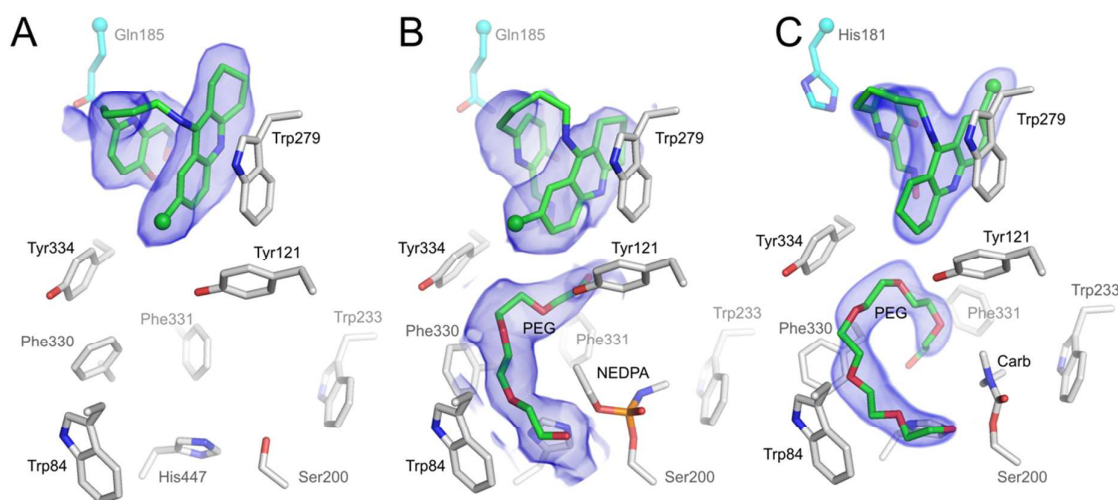


Figure 5 Crystal structures of unmodified *TcAChE* and of its conjugates complexed with **2**. Volume represents feature enhanced maps (fem) contoured at 1σ . A) *TcAChE*-**2** complex (pdb 6g4n). One copy of **2** is seen at the PAS, while the active site is empty; B) NEDPA-*TcAChE*-**2** complex (pdb 6g4p). A copy of **2** is seen, at the PAS, and a PEG oligomer from the crystallization conditions is seen alongside the phosphyl moiety; C) Carbamyl-*TcAChE*-**2** (pdb 6fqm). A copy of **2** is clearly present at the PAS, while, again, a PEG oligomer is adjacent to the carbamyl moiety. The binding orientation of **2** at the PAS in the 3 panels is stabilized by Gln185 or His181 (cyan) of a symmetry mate specific of the crystal packing, thus partially artefactual.

We solved the structure of the NEDPA-*TcAChE*-**2** ternary complex by successively soaking *TcAChE* crystal first in NEDPA, and then in **2**, as had been done for **1** (Figure 5B). The

1
2
3 structure is very similar to that observed for the ternary complex of **1** with respect to the copy
4 of reactivator binding at the PAS. However, no copy of **2** is present at the bottom of the gorge
5 where the phosphyl adduct stabilizes a PEG molecule. The copy of **2** bound at the PAS is in
6 the same orientation as in the non-phosphylated *TcAChE-2* complex in both monomers A and
7 B, thus confirming the affinity of **2** for the PAS of the inhibited enzyme.
8
9

10
11
12 The same holds true for the carbamyl-*TcAChE-2* ternary complex (Figure 5C), which is
13 virtually identical to carbamyl-*TcAChE-1*, except that the orientation of the tacrine moiety
14 can be unambiguously assigned due to the presence of the chlorine substituent.
15
16
17
18
19

20 21 **Conclusion**

22
23
24 We present the crystal structure of the complex of *TcAChE* with the reactivator, **1**, which
25 reveals a binding conformation within the active site that can account for its sub-millimolar
26 inhibition of the enzyme. While AChE inhibition could protect against OP intoxication by
27 transiently masking the active site from nerve agent ²⁸, we developed a new molecule with
28 the intention of limiting binding to the PAS, in a position which would permit favourable
29 interaction of the aldoxime moiety with the covalently bound phosphyl group. To this end, **2**,
30 bearing a chlorine at position 7 of the tacrine moiety was designed and tested by molecular
31 docking before being synthesized. As predicted, the *in vitro* reactivation capability of **2** is
32 comparable to that of **1**, but it is a 10-fold weaker inhibitor. Crystallographic data confirmed
33 that it could bind only at the PAS of native *TcAChE*, while preserving the same binding
34 mode as **1** in the OP conjugates. The data presented demonstrate the value of rational design
35 in refining the chemical structures of reactivator candidates, and support further investigation
36 of **2** for *in vivo* evaluation studies.
37
38
39
40
41
42
43
44
45
46
47
48
49
50
51
52
53
54
55
56
57
58
59
60

Experimental Section

1. Chemicals

Chemicals including paraoxon were purchased from Sigma-Aldrich unless mentioned otherwise. The tabun analog, 4-nitrophenyl ethyl dimethylphosphoramidate (NEDPA), and the sarin surrogate 4-nitrophenyl isopropyl methylphosphonate (NIMP), were synthesized by Catherine Gomez (COBRA laboratory, UMR 6014, France) as described²⁶. Stock solutions of 5 mM VX and tabun in isopropanol were obtained from DGA maîtrise NRBC (Vert le Petit, France). **1** was synthesized as previously published¹⁵. **2** was synthesized as described in the result section with details and analyses reported in the supplementary information file. Compound **1** and **2** were $\geq 95\%$ pure as determined by HPLC and HRMS. They are water-soluble at concentrations up to 40 mM (higher concentration not tested). The rivastigmine analog was a gift from Ben Ross from the University of Queensland, synthesized by Satish Dighe (unpublished structure ; (S)-3-(1-(dimethylamino)ethyl)-5-hydroxy-phenyl ethyl(methyl)carbamate).

2. AChE preparations

Recombinant hAChE was produced and purified as previously described²². The G₂ form of TcAChE was purified from electric organ tissue of *Torpedo californica*²⁹.

3. Inhibition measurements

Oximes were dissolved in MeOH to make 5 or 10 mM stock solution. Recombinant hAChE activity was measured spectrophotometrically at 25 °C, monitoring absorbance at 412 nm, in 1 mL Ellman's buffer (0.5 mM DTNB/0.1% BSA/5% MeOH/0.1 M phosphate, pH 7.4), in the presence of appropriate oxime concentrations. Measurements were performed at least in duplicate for each concentration tested. The oxime concentration producing 50% inhibition

was determined by non-linear fitting with ProFit (Quantumsoft) using the standard IC_{50} equation: $\%Activity = 100 \cdot IC_{50} / (IC_{50} + [Ox])$.

4. Reactivation of hAChE inhibited by OPs

The inhibition of 120 μ M hAChE was performed with a 5-fold excess of OP, in 0.1% BSA/20 mM Tris, pH 7.4, at 25 °C. After a 20-min incubation, the inhibited hAChE was desalted on a PD-10 column (GE Healthcare).

2-PAM and obidoxime chloride were from Sigma (Saint-Quentin Fallavier, France) and HI-6 from Pharmacie Centrale des Armées (Orléans, France). OP-inhibited hAChE was incubated at 37°C with at least four concentrations of the oxime in 0.1% BSA/0.1 M phosphate, pH 7.4. The final concentration of MeOH in the incubation mixture was <2%, and had no influence on the enzyme's activity. At time intervals of from 1-10 min, depending on the reactivation rate, 10- μ L aliquots were transferred to cuvettes containing 1mM acetylthiocholine in 1 mL Ellman's buffer, for measurement of hAChE activity at 25 °C. The enzyme activity in the control, *viz.*, uninhibited enzyme + oxime, remained constant throughout the experiment. Oximolysis was undetectable.

The percentage of reactivated enzyme ($\%E_{react}$) was calculated as the ratio of the recovered enzyme activity and the activity in the control. The apparent reactivation rate, k_{obs} , for each oxime concentration, the dissociation constant, K_D , of inhibited enzyme-oxime complex (E-POx), and the reactivation rate constant, k_r , were calculated by non-linear fit with ProFit (Quantumsoft) using the standard oxime concentration-dependent reactivation equation derived from the following scheme:



$$\%E_{react} = 100 \cdot (1 - e^{-k_{obs} \cdot t}) \quad \text{and} \quad k_{obs} = \frac{k_r [Ox]}{K_D + [Ox]}$$

1
2
3 The reactivator concentrations used for each set of experiments are given in the
4
5 Supplementary Information.
6

7 8 **5. Molecular docking**

9
10 Flexible docking was performed using AutoDock Vina³⁰ as described before¹⁵. Briefly, the
11
12 system was prepared in PyMOL (Schrödinger) using the plug-in developed by Daniel
13
14 Seeliger (<http://wwwuser.gwdg.de/~dseelig/adplugin.html>). VX-hAChE was constructed
15
16 from the apo form (pdb code 4ey4) by homology with the mAChE-VX structure (pdb code
17
18 2y2u), retaining in the active site all the usually conserved water molecules³¹. Residues in the
19
20 gorge (Tyr72, Asp74, Trp86, Tyr124, Ser125, Trp286, Tyr337, Phe338, Tyr341; hAChE
21
22 numbering) were selected as flexible, along with the ethyl group of VX. A 60 × 60 × 60 Å
23
24 docking box was employed, centered near the bottom of the gorge, between Tyr124 and
25
26 Trp86. Ligands were built and optimized from SMILES string using phenix eLBOW³². The
27
28 default parameter set of AutoDock Vina was used to generate 9 docking poses per molecule.
29
30 The pose with the best energy score was selected as the most representative.
31
32

33 34 **6. X-ray crystallography**

35
36 Crystallization of *TcAChE* utilized ~36% PEG200/150 mM MES, pH 5.6. The optimal
37
38 concentration of PEG200 was determined for each batch of purified enzyme, and was in the
39
40 range of 30-38%. Most crystals were of the orthorhombic form with only very few trigonal
41
42 crystals among them. Trigonal crystals are usually of better quality and were used in priority
43
44 when available. In both forms, a symmetric molecule faces the active site gorge entrances
45
46 without occluding it, and surface residues Gln185 and His181 can eventually interact with
47
48 PAS ligands.
49

50
51 To obtain tabun and NEDPA conjugates, the crystals were soaked in mother liquor containing
52
53 500 μM OP diluted in water from the stock solution. The affinities of the OPs for the enzyme,
54
55 and their reactivities, are very high, so inhibition of the crystalline *TcAChE* is limited mainly
56
57
58
59
60

1
2
3 by the diffusion of the OP into the solvent channels. The soaking of neutral reactivators **1** and
4
5 **2** was performed at a concentration of 20 mM in dimethylsulfoxide (DMSO) at room
6
7 temperature and subsequently diluting them in crystal mother liquor to a final concentration
8
9 of 1mM. Soaking was times ranging from 2 min to 2 days were tested. The ternary
10
11 complexes, *TcAChE*-NEDPA-**1** and *TcAChE*-NEDPA-**2**, were obtained by an initial soak of
12
13 a few minutes with NEDPA, using the protocol described above, followed by a second one in
14
15 a solution containing 1mM of reactivator and 500 μ M OP to maintain the enzyme in a
16
17 phosphorylated state. Similarly, the ternary complexes carbamyl-*TcAChE*- **1** and carbamyl-
18
19 *TcAChE*-**2** were obtained by an initial soak of a few minutes in mother liquor containing 500
20
21 μ M of the rivastigmine analog, followed by a second soak in a solution containing 1mM of
22
23 reactivator and 500 μ M of the analog.
24
25

26
27 *TcAChE* crystals can be cryo-cooled without further cryo-protection due to the presence of
28
29 PEG200 in the crystallisation conditions. Diffraction data were collected at the ESRF, on MX
30
31 beamlines ID14-4, ID23-1 and ID29^{33, 34}, following the most appropriate strategy suggested
32
33 by EDNA³⁵. Datasets were either processed with XDS³⁶ or using the automatic processing
34
35 output provided by the ESRF. Once the data had been scaled and truncated at a proper
36
37 resolution, using the aimless-pointless pipeline in CCP4, native *TcAChE* monomer (PDB
38
39 entry 1ea5) was used as a starting model for molecular replacement by Phaser³⁷. The
40
41 resulting model was completed by iterative refinement in phenix.refine³⁸ and manual
42
43 building with Coot³⁹. Ligand models were built using phenix.eLBOW³².
44
45
46
47

48 *Supplementary information* Detailed experimental procedures for the synthesis of **2** and
49
50 analyses, reactivation kinetics for **1** and **2**, and clinically relevant concentrations of 2-PAM,
51
52 HI-6, obidoxime, **1** and **2**. Molecular Formula Strings are available.
53
54
55
56
57
58
59
60

1
2
3 *PDB ID Codes:* Tabun-*TcAChE* conjugate, 6g17; *TcAChE-1*, 6g4n; NEDPA-*TcAChE-1*,
4 6g4o; *TcAChE-2*, 6g4m; NEDPA-*TcAChE-2*, 6g4p. Authors will release the atomic
5 coordinates upon article publication.
6
7

8
9
10 *Corresponding Author Information.* Département de Toxicologie et Risques Chimiques,
11 Institut de Recherche Biomédicale des Armées, 1 place du Général Valérie André, BP73,
12 91223 Brétigny-sur-Orge, France ; Tel.: +33(0)178651877 ; email :
13
14
15
16
17 florian.nachon@chemdef.fr
18

19
20 *Author Contribution.* §These authors contributed equally to this work. GS, EdIM and FN
21 performed X-ray crystallography. GS and FN performed docking. JdS synthesized compound
22 **1** and **2** under the supervision of RCDB and RB. JD and FN provided hAChE and performed
23 the inhibition and reactivation kinetics. JLS and IS provided *TcAChE*. All authors contributed
24 to the writing and improvement of the manuscript.
25
26
27
28
29

30
31
32 *Acknowledgement.* GS and EdIM were supported by Direction Générale de l'Armement
33 (DGA) through a grant from the ANR ASTRID program (ReCNSAChE). FN and JD were
34 funded by the French Ministry of Armed Forces (DGA and SSA). JDS gratefully
35 acknowledge the DGA, the Defence Science and Technology Laboratory (DSTL), UK, and
36 the Centre National de la Recherche Scientifique (CNRS) for a research grant. The University
37 of Strasbourg and the University of Southampton are also acknowledged for their support.
38 We thank the ESRF staff for help during data collection.
39
40
41
42
43
44
45
46

47
48 *Notes.* The authors declare no competing financial interest.
49

50
51 *Abbreviations used:* AChE, acetylcholinesterase; *TcAChE*, *Torpedo californica*
52 acetylcholinesterase; BBB, blood-brain barrier; CAS, catalytic aromatic site; PAS, peripheral
53 aromatic site; PEG, polyethylene glycol
54
55
56
57
58
59
60

References

1. Silman, I.; Sussman, J. L. Acetylcholinesterase: 'classical' and 'non-classical' functions and pharmacology. *Curr. Opin. Pharmacol.* **2005**, *5*, 293-302.
2. Mercey, G.; Verdelet, T.; Renou, J.; Kliachyna, M.; Baati, R.; Nachon, F.; Jean, L.; Renard, P. Y. Reactivators of acetylcholinesterase inhibited by organophosphorus nerve agents. *Acc. Chem. Res.* **2012**, *45*, 756-766.
3. Sharma, R.; Gupta, B.; Singh, N.; Acharya, J. R.; Musilek, K.; Kuca, K.; Ghosh, K. K. Development and Structural Modifications of Cholinesterase Reactivators against Chemical Warfare Agents in Last Decade: A Review. *Mini Rev. Med. Chem.* **2015**, *15*, 58-72.
4. Sakurada, K.; Matsubara, K.; Shimizu, K.; Shiono, H.; Seto, Y.; Tsuge, K.; Yoshino, M.; Sakai, I.; Mukoyama, H.; Takatori, T. Pralidoxime iodide (2-PAM) penetrates across the blood-brain barrier. *Neurochem. Res.* **2003**, *28*, 1401-1407.
5. Worek, F.; Thiermann, H.; Szinicz, L.; Eyer, P. Kinetic analysis of interactions between human acetylcholinesterase, structurally different organophosphorus compounds and oximes. *Biochem. Pharmacol.* **2004**, *68*, 2237-2248.
6. Lorke, D. E.; Kalasz, H.; Petroianu, G. A.; Tekes, K. Entry of oximes into the brain: a review. *Curr. Med. Chem.* **2008**, *15*, 743-753.
7. Barckow, D.; Neuhaus, G.; Erdmann, W. D. Treatment of parathion (E 605) poisoning with the cholinesterase-reactivating substance obidoxime (Toxogonin). *Arch. Toxikol.* **1969**, *24*, 133-146.
8. Clement, J. G.; Lockwood, P. A. HI-6, an oxime which is an effective antidote of soman poisoning: a structure-activity study. *Toxicol. Appl. Pharmacol.* **1982**, *64*, 140-146.

- 1
2
3 9. Oldiges, H.; Schoene, K. Pyridinium and imidazolium salts as antidotes for soman
4 and paraoxon poisoning in mice. *Arch. Toxikol.* **1970**, *26*, 293-305.
5
6
- 7 10. Schoene, K.; Steinhanses, J.; Oldiges, H. Reactivation of soman inhibited
8 acetylcholinesterase in vitro and protection against soman in vivo by
9 bispyridinium-2-aldoximes. *Biochem. Pharmacol.* **1983**, *32*, 1649-1651.
10
11
- 12 11. Sussman, J. L.; Harel, M.; Frolow, F.; Oefner, C.; Goldman, A.; Toker, L.; Silman, I.
13 Atomic structure of acetylcholinesterase from *Torpedo californica*: a prototypic
14 acetylcholine-binding protein. *Science* **1991**, *253*, 872-879.
15
16
- 17 12. Kryger, G.; Harel, M.; Giles, K.; Toker, L.; Velan, B.; Lazar, A.; Kronman, C.; Barak, D.;
18 Ariel, N.; Shafferman, A.; Silman, I.; Sussman, J. L. Structures of recombinant native
19 and E202Q mutant human acetylcholinesterase complexed with the snake-venom
20 toxin fasciculin-II. *Acta Crystallogr. D Biol. Crystallogr.* **2000**, *56*, 1385-1394.
21
22
- 23 13. Ekstrom, F.; Hornberg, A.; Artursson, E.; Hammarstrom, L. G.; Schneider, G.; Pang,
24 Y. P. Structure of HI-6*sarin-acetylcholinesterase determined by X-ray
25 crystallography and molecular dynamics simulation: reactivator mechanism and
26 design. *PLoS ONE* **2009**, *4*, e5957.
27
28
- 29 14. Ekstrom, F.; Pang, Y. P.; Boman, M.; Artursson, E.; Akfur, C.; Borjegen, S. Crystal
30 structures of acetylcholinesterase in complex with HI-6, Ortho-7 and obidoxime:
31 structural basis for differences in the ability to reactivate tabun conjugates.
32
33
34
35
36
37
38
39
40
41
42
43
44
45
46
- 47 15. Kliachyna, M.; Santoni, G.; Nussbaum, V.; Renou, J.; Sanson, B.; Colletier, J. P.;
48 Arboleas, M.; Loiodice, M.; Weik, M.; Jean, L.; Renard, P. Y.; Nachon, F.; Baati, R.
49 Design, synthesis and biological evaluation of novel tetrahydroacridine pyridine-
50 aldoxime and -amidoxime hybrids as efficient uncharged reactivators of nerve
51 agent-inhibited human acetylcholinesterase. *Eur. J. Med. Chem.* **2014**, *78*, 455-467.
52
53
54
55
56
57
58
59
60

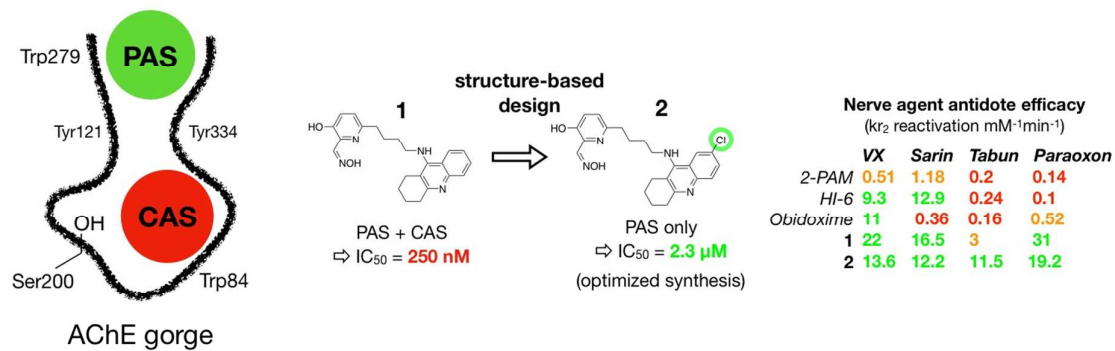
- 1
2
3 16. Korabecny, J.; Musilek, K.; Zemek, F.; Horova, A.; Holas, O.; Nepovimova, E.;
4 Opletalova, V.; Hroudova, J.; Fisar, Z.; Jung, Y. S.; Kuca, K. Synthesis and in vitro
5 evaluation of 7-methoxy-N-(pent-4-enyl)-1,2,3,4-tetrahydroacridin-9-amine-new
6 tacrine derivate with cholinergic properties. *Bioorg. Med. Chem. Lett.* **2011**, *21*,
7 6563-6566.
8
9
10
11
12
13
14 17. Kuca, K.; Juna, D.; Musilek, K. Structural requirements of acetylcholinesterase
15 reactivators. *Mini Rev. Med. Chem.* **2006**, *6*, 269-277.
16
17
18 18. de Sousa, J.; Brown, R. C. D.; Baati, R. Buchwald-Hartwig Amination Approach for
19 the Synthesis of Functionalized 1,2,3,4-Tetrahydroacridine Derivatives. *Eur. J. Org.*
20 *Chem.* **2014**, 2014, 3468-3474.
21
22
23
24
25 19. Cross, R. M.; Maignan, J. R.; Mutka, T. S.; Luong, L.; Sargent, J.; Kyle, D. E.; Manetsch,
26 R. Optimization of 1,2,3,4-tetrahydroacridin-9(10H)-ones as antimalarials utilizing
27 structure-activity and structure-property relationships. *J. Med. Chem.* **2011**, *54*,
28 4399-4426.
29
30
31
32
33
34 20. Renou, J.; Loiodice, M.; Arboleas, M.; Baati, R.; Jean, L.; Nachon, F.; Renard, P. Y.
35 Tryptoline-3-hydroxypyridinaldoxime conjugates as efficient reactivators of
36 phosphylated human acetyl and butyrylcholinesterases. *Chem. Commun. (Camb.)*
37 **2014**, *50*, 3947-3950.
38
39
40
41
42
43 21. Carletti, E.; Colletier, J. P.; Dupeux, F.; Trovaslet, M.; Masson, P.; Nachon, F.
44 Structural evidence that human acetylcholinesterase inhibited by tabun ages
45 through O-dealkylation. *J. Med. Chem.* **2010**, *53*, 4002-4008.
46
47
48
49 22. Carletti, E.; Li, H.; Li, B.; Ekstrom, F.; Nicolet, Y.; Loiodice, M.; Gillon, E.; Froment, M.
50 T.; Lockridge, O.; Schopfer, L. M.; Masson, P.; Nachon, F. Aging of cholinesterases
51 phosphylated by tabun proceeds through O-dealkylation. *J. Am. Chem. Soc.* **2008**,
52 *130*, 16011-16020.
53
54
55
56
57
58
59
60

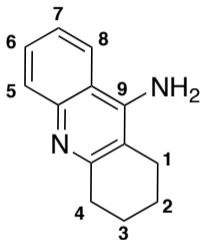
- 1
2
3 23. Millard, C. B.; Kryger, G.; Ordentlich, A.; Greenblatt, H. M.; Harel, M.; Raves, M. L.;
4
5 Segall, Y.; Barak, D.; Shafferman, A.; Silman, I.; Sussman, J. L. Crystal structures of
6
7 aged phosphonylated acetylcholinesterase: nerve agent reaction products at the
8
9 atomic level. *Biochemistry* **1999**, 38, 7032-7039.
10
11
12 24. Dym, O.; Song, W.; Felder, C.; Roth, E.; Shnyrov, V.; Ashani, Y.; Xu, Y.; Joosten, R. P.;
13
14 Weiner, L.; Sussman, J. L.; Silman, I. The impact of crystallization conditions on
15
16 structure-based drug design: A case study on the methylene
17
18 blue/acetylcholinesterase complex. *Protein Sci.* **2016**, 25, 1096-1114.
19
20
21 25. Harel, M.; Schalk, I.; Ehret-Sabatier, L.; Bouet, F.; Goeldner, M.; Hirth, C.; Axelsen, P.
22
23 H.; Silman, I.; Sussman, J. L. Quaternary ligand binding to aromatic residues in the
24
25 active-site gorge of acetylcholinesterase. *Proc. Natl. Acad. Sci. U. S. A.* **1993**, 90,
26
27 9031-9035.
28
29
30 26. Meek, E. C.; Chambers, H. W.; Coban, A.; Funck, K. E.; Pringle, R. B.; Ross, M. K.;
31
32 Chambers, J. E. Synthesis and in vitro and in vivo inhibition potencies of highly
33
34 relevant nerve agent surrogates. *Toxicol. Sci.* **2012**, 126, 525-533.
35
36
37 27. Ellman, G. L.; Courtney, K. D.; Andres, V., Jr.; Feather-Stone, R. M. A new and rapid
38
39 colorimetric determination of acetylcholinesterase activity. *Biochem. Pharmacol.*
40
41 **1961**, 7, 88-95.
42
43 28. Lallement, G.; Baille, V.; Baubichon, D.; Carpentier, P.; Collombet, J. M.; Filliat, P.;
44
45 Foquin, A.; Four, E.; Masqueliez, C.; Testylier, G.; Tonduli, L.; Dorandeu, F. Review
46
47 of the value of huperzine as pretreatment of organophosphate poisoning.
48
49 *Neurotoxicology* **2002**, 23, 1-5.
50
51
52 29. Sussman, J. L.; Harel, M.; Frolow, F.; Varon, L.; Toker, L.; Futerman, A. H.; Silman, I.
53
54 Purification and crystallization of a dimeric form of acetylcholinesterase from
55
56
57
58
59
60

- 1
2
3 Torpedo californica subsequent to solubilization with phosphatidylinositol-
4 specific phospholipase C. *J. Mol. Biol.* **1988**, 203, 821-823.
5
6
7 30. Trott, O.; Olson, A. J. AutoDock Vina: improving the speed and accuracy of docking
8 with a new scoring function, efficient optimization, and multithreading. *J. Comput.*
9 *Chem.* **2010**, 31, 455-461.
10
11
12 31. Koellner, G.; Kryger, G.; Millard, C. B.; Silman, I.; Sussman, J. L.; Steiner, T. Active-
13 site gorge and buried water molecules in crystal structures of acetylcholinesterase
14 from Torpedo californica. *J. Mol. Biol.* **2000**, 296, 713-735.
15
16
17 32. Moriarty, N. W.; Grosse-Kunstleve, R. W.; Adams, P. D. electronic Ligand Builder
18 and Optimization Workbench (eLBOW): a tool for ligand coordinate and restraint
19 generation. *Acta Crystallogr. D Biol. Crystallogr.* **2009**, 65, 1074-1080.
20
21
22 33. de Sanctis, D.; Beteva, A.; Caserotto, H.; Dobias, F.; Gabadinho, J.; Giraud, T.; Gobbo,
23 A.; Guijarro, M.; Lentini, M.; Lavault, B.; Mairs, T.; McSweeney, S.; Petitdemange, S.;
24 Rey-Bakaikoa, V.; Surr, J.; Theveneau, P.; Leonard, G. A.; Mueller-Dieckmann, C.
25 ID29: a high-intensity highly automated ESRF beamline for macromolecular
26 crystallography experiments exploiting anomalous scattering. *J. Synchrotron*
27 *Radiat.* **2012**, 19, 455-461.
28
29
30 34. Nurizzo, D.; Mairs, T.; Guijarro, M.; Rey, V.; Meyer, J.; Fajardo, P.; Chavanne, J.;
31 Biasci, J. C.; McSweeney, S.; Mitchell, E. The ID23-1 structural biology beamline at
32 the ESRF. *J. Synchrotron Radiat.* **2006**, 13, 227-238.
33
34
35 35. Incardona, M. F.; Bourenkov, G. P.; Levik, K.; Pieritz, R. A.; Popov, A. N.; Svensson, O.
36 EDNA: a framework for plugin-based applications applied to X-ray experiment
37 online data analysis. *J. Synchrotron Radiat.* **2009**, 16, 872-879.
38
39
40 36. Kabsch, W. XDS. *Acta Crystallogr. D Biol. Crystallogr.* **2010**, 66, 125-132.
41
42
43
44
45
46
47
48
49
50
51
52
53
54
55
56
57
58
59
60

- 1
2
3 37. McCoy, A. J.; Grosse-Kunstleve, R. W.; Adams, P. D.; Winn, M. D.; Storoni, L. C.; Read,
4 R. J. Phaser crystallographic software. *J. Appl. Crystallogr.* **2007**, 40, 658-674.
5
6
7 38. Adams, P. D.; Afonine, P. V.; Bunkoczi, G.; Chen, V. B.; Davis, I. W.; Echols, N.; Headd,
8 J. J.; Hung, L. W.; Kapral, G. J.; Grosse-Kunstleve, R. W.; McCoy, A. J.; Moriarty, N. W.;
9 Oeffner, R.; Read, R. J.; Richardson, D. C.; Richardson, J. S.; Terwilliger, T. C.; Zwart,
10 P. H. PHENIX: a comprehensive Python-based system for macromolecular
11 structure solution. *Acta Crystallogr. D Biol. Crystallogr.* **2010**, 66, 213-221.
12
13
14 39. Emsley, P.; Lohkamp, B.; Scott, W. G.; Cowtan, K. Features and development of
15 Coot. *Acta Crystallogr. D Biol. Crystallogr.* **2010**, 66, 486-501.
16
17
18
19
20
21
22
23
24
25
26
27
28
29
30
31
32
33
34
35
36
37
38
39
40
41
42
43
44
45
46
47
48
49
50
51
52
53
54
55
56
57
58
59
60

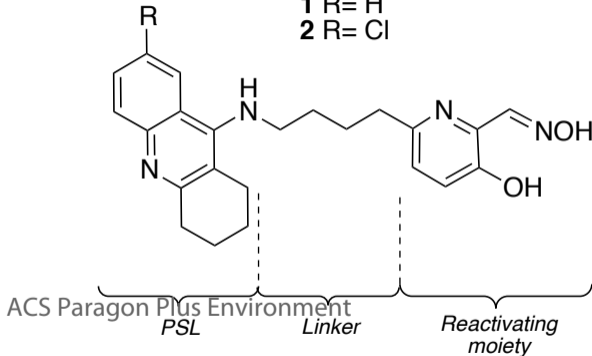
Table of Contents Graphic

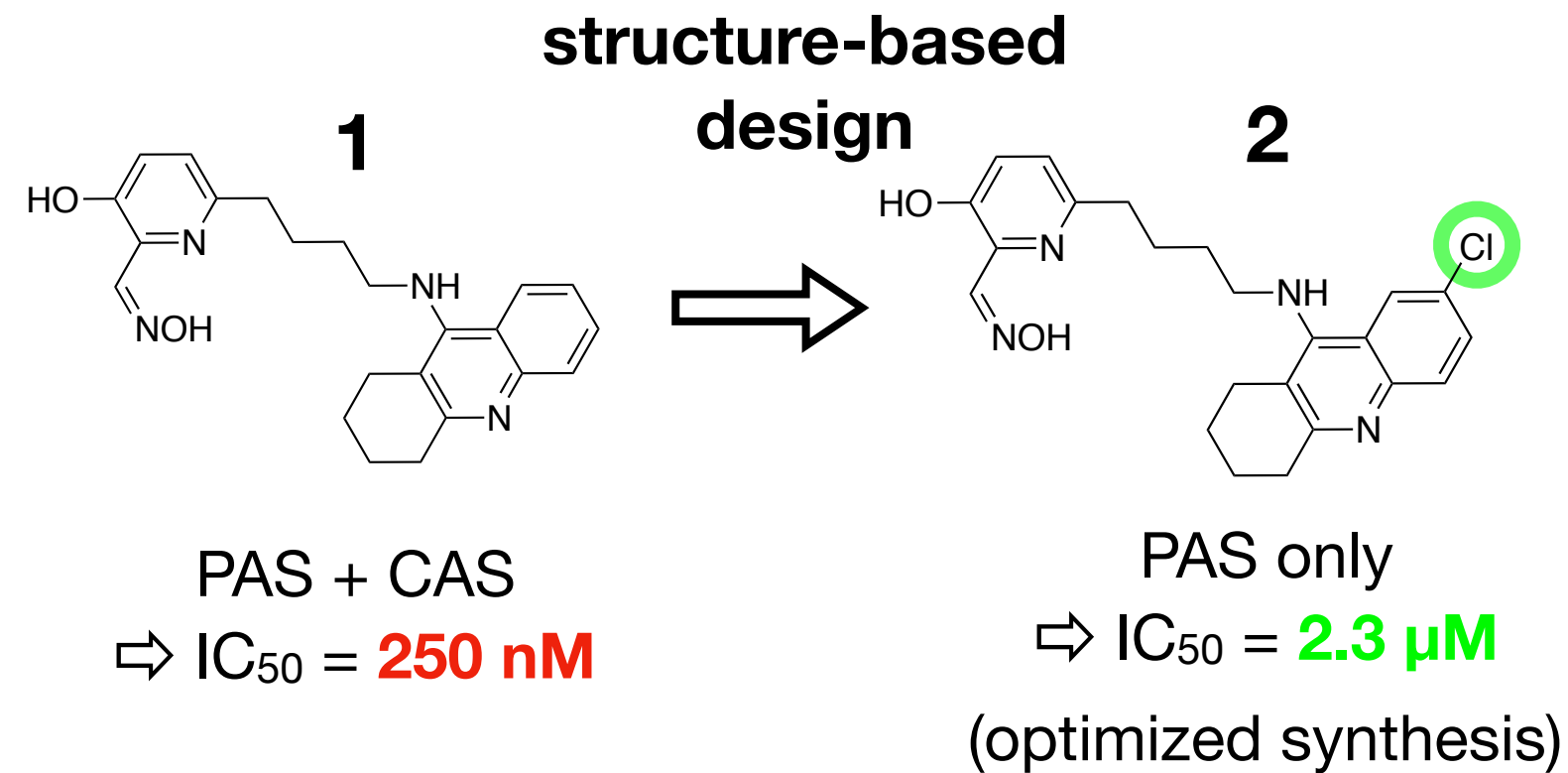
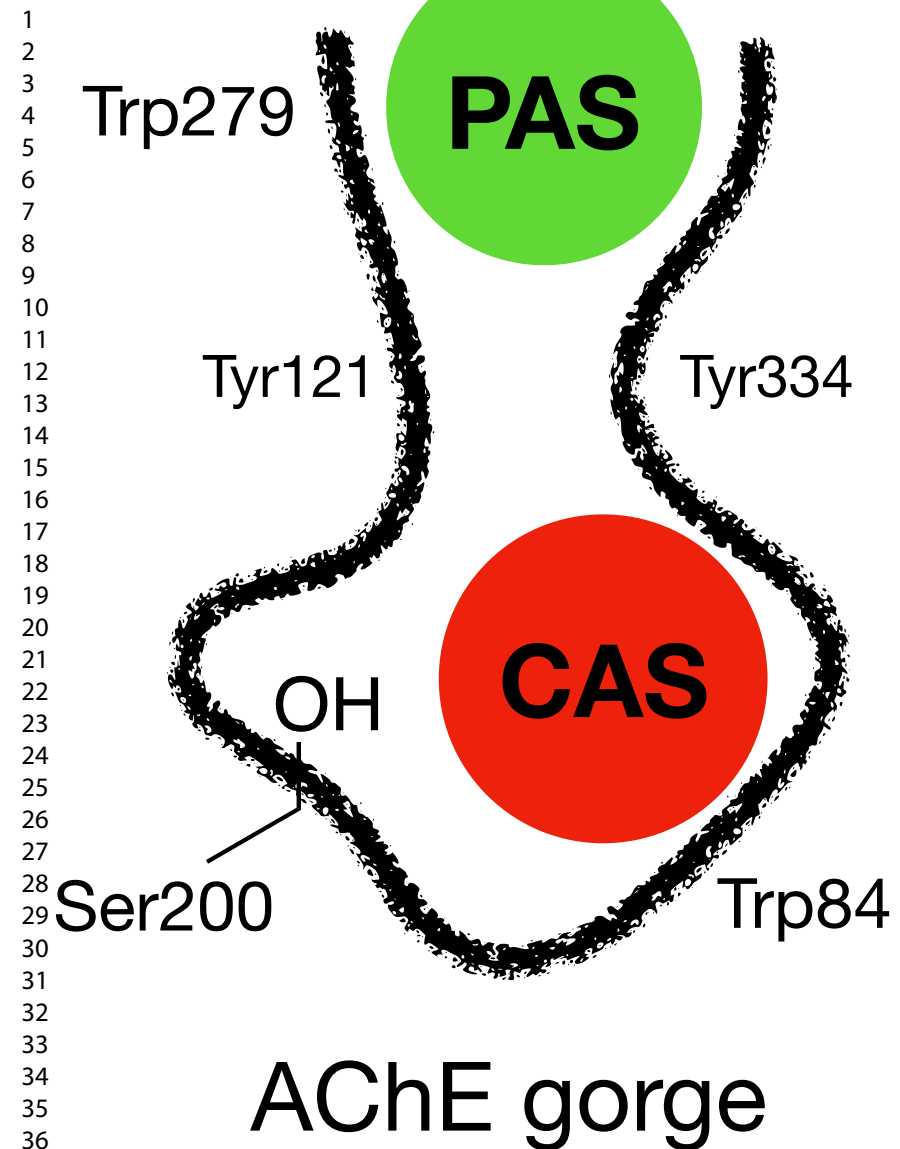




Tacrine
Cognex®

1 R= H
2 R= Cl





Nerve agent antidote efficacy
(kr₂ reactivation mM⁻¹min⁻¹)

	VX	Sarin	Tabun	Paraoxon
<i>2-PAM</i>	0.51	1.18	0.2	0.14
<i>HI-6</i>	9.3	12.9	0.24	0.1
<i>Obidoxime</i>	11	0.36	0.16	0.52
1	22	16.5	3	31
2	13.6	12.2	11.5	19.2